MANUFACTURING MULTI-MATRIX COMPOSITES: OUT-OF-VACUUM BAG CONSOLIDATION

Arjun Radhakrishnan
Bristol Composites Institute, University of Bristol,
Bristol, BS8 1TR, UK
arjun.radhakrishnan@bristol.ac.uk

Ioannis Georgillas
Department of Mechanical Engineering, University of Bath,
Bath, BA2 7AY, UK
I.Georgilas@bath.ac.uk

Ian Hamerton
Bristol Composites Institute, University of Bristol,
Bristol, BS8 1TR, UK
Ian.hamerton@bristol.ac.uk

Milo S.P. Shaffer
Department of Chemistry and Department of Materials, Imperial College London,
London SW7 2AZ, UK
m.shaffer@imperial.ac.uk

Dmitry S Ivanov
Bristol Composites Institute, University of Bristol,
Bristol, BS8 1TR, UK
dmitry.ivanov@bristol.ac.uk

ABSTRACT

The formation of porosity is a major challenge in any composite manufacturing process, particularly in the absence of vacuum assistance. Highly localised injection of polymer matrix into regions of interest in a dry preform is a route to manufacturing multi-matrix fibre-reinforced composites with high filler concentrations, which are otherwise difficult to achieve. Unlike traditional composites, such multi-matrix fibre-reinforced composite systems, which combine multiple resins in continuous form, offer improved structural performance around stress concentrators and multifunctional capabilities. As the process lacks

vacuum assistance, porosity becomes a primary issue to be addressed. This paper presents a rheo-kinetic coupled rapid consolidation procedure for optimising the quality of localised matrix patches. The procedure involves manufacturing trials and analytical consolidation models to determine the best processing program for minimal voidage in the patch. The results provide a step towards an efficient manufacturing process for the optimal design of multi-matrix composites without the need for complex vacuum bag arrangements, thus reducing cost and time while opening avenues to improve overall composite performance.

Keywords: Multi-matrix composites; Analytical modelling of resin flow; Voids; Matrix hybridisation.

1. INTRODUCTION

Composites already deliver state-of-the-art structural performance by combining reinforcing fibres with polymer matrices. There is growing interest in hybridising various constituents into one coherent composite system to improve structural performance, confer multifunctional properties and improve manufacturability. Several reviews compile and detail the hybridisation of different fibres within the fibre bundles and at the ply scale [1], or as continuous or discrete sub-reinforcements [2], and hierarchical composites have been explored via the introduction of micro- or nano-scale additives within the matrix [3,4]. However, there is growing evidence that the combination of various matrices in one multi-matrix system opens a new range of opportunities for fibre composite design. Recent studies have demonstrated that multi-matrix composites can enhance the dimensional stability of preforms [5], mitigate defects during forming [6], integrate electrically conductive areas [7], improve structural performance around stress concentrators [8], and provide containment for functional zones [9].

Among the various routes for combining matrices [10,11], local injection is particularly appealing as it facilitates: (a) the selective introduction of resin into critical areas and (b) high additive loadings, which may be too viscous to process using conventional liquid composite moulding (LCM) processes. In this process, a fixed quantity of resin is injected directly into the textile preform using a needle without confining the area of impregnation—multiple consecutive injections through the thickness of the laminate result in impregnation of the area around the injection. Subsequently, the impregnated region is consolidated and cured to form a composite patch hosted within a continuous dry reinforcement. The larger dry preform outside the patch can then be infused with a second resin to form a multi-matrix composite system. The localised injection process does not involve vacuum assistance, which, when combined with the dual-scale flow, leads to air entrapment resulting in locked-in porosity within the composite patch.

The mechanisms of void entrapment have been very well studied in the context of the classical (non-vacuum-assisted) resin transfer moulding (RTM) processes [12]. The drastic difference in channel sizes within and outside fibre bundles leads to two pre-dominant flow types with contrasting speeds between these two domains. At low injection speeds, the capillary pressure dominates over viscous stresses in fibre-free channels, which leads to large inter-bundle voids. At high injection speeds, the flow ratio is reversed, and the micro-scale voids occur within intra-yarn spaces [13]. In non-vacuum-assisted liquid composite moulding (LCM) processes, this problem may be partially mitigated by tuning the injection flow rate to balance the intra-yarn and inter-

yarn speeds. However, in a local injection process, the situation is different. The resin is driven through the nozzle/needle perpendicular to the plane of the laminate, and capillary forces then spread the resin in-plane within the yarns, leading to considerable void entrapment in the inter-yarn space [5]. The in-plane flow velocity is hence not determined by the flow rate at the inlet, and the occurrence of voids is inevitable at the injection stage. Mitigating voids during consolidation may be a better option. The right choice of consolidation strategy is known to reduce both the size and quantity of the voids produced in material systems, such as thermosetting prepregs [14] and thermoplastic precursors [15], although the mechanisms of void suppression may be different. In thermoplastics [16] or high-viscosity thermoset prepregs [17], the roughness of the inter-ply region forms resin filaments, which are then squeezed to fill the void. In LCM processes, the voids can be suppressed by building up pressure in resin that overcomes surface tension, viscous forces, and pressure of entrapped air to reduce the size of the void or even force the air to dissolve in the resin [18].

Mechanics of concurrent flow and deformation process is relatively well understood in the context of compression resin transfer moulding [19], consolidation with bleeder [20] or a variety of mechanisms occurring in toughened prepregs [21,22]. To be effective, the total applied consolidation pressure must be shared between the resin and the fibre network. Increasing the externally applied consolidation pressure may not necessarily lead to an increase in the resin pressure. If the resin viscosity is low, and there is room for the resin to bleed out of the fibre system, the load may be carried by the fibre network while the resin pressure decays to zero [23]; on the other hand,

higher viscosity systems exhibit lower porosity in comparable conditions [24]. Hence, a promising approach for a thermosetting resin is to advance the degree of cure (DOC), which increases the viscosity and thus enables the resin to carry an increased fraction of the applied consolidation load.

The rheo-kinetics of the resin is, therefore, key to the elimination of voidage and must be understood to develop a suitable consolidation programme, closely linking the resin viscosity to the time of application of consolidation pressure. The viscosity of a thermosetting resin during thermal treatment is affected primarily by two competing phenomena: a) increased crosslinking of the molecules to form larger molecular networks and b) increased molecular mobility [25] due to the increase in available thermal energy [26]. The earliest models for viscosity evolution addressed the various processing and material aspects such as non-isothermal thermal history [27], temperature and rate dependence [28], and evolution of the glass-transition temperature in thermosets [29,30]. A widely used model initially developed for polyurethanes utilises a combination of isothermal viscosity measurements and a cure-kinetic model to predict the evolution of viscosity [31]. An alternative route for epoxies was pursued by Kiuna *et al.* [32], who expressed the rheo-kinetic model in the form of a differential equation like the well-established expression for cure-kinetics:

$$\frac{d\beta}{dt} = \frac{k(T)}{g(\beta)} \tag{1}$$

where $\beta = ln\left(\frac{\eta(T,t)}{\eta_0(T)}\right)$ is the non-dimensional viscosity, η and η_0 are the current and initial viscosities in isothermal conditions and the normalised time, $g(\beta)$, is a

function of normalised viscosity that is derived from the experimental data, the term $k(T)$ is an empirical function showing the cure rate advance for a given temperature, *T.* The model has been shown to fit a range of resin systems from epoxies to polyurethane at low DOC [32–34] and appeared to be applicable for fast-curing resin systems [35,36].

In the current process to mitigate the defects, it is critical to understand the relation between the consolidation process and the mechanisms by which the resin flows through the preform because of this consolidation. The identification of the flow mechanisms presents a certain challenge, as multiple flow processes may occur simultaneously, and the description of each requires fundamentally different material characterisation and constitutive equations. This study explores the benefits of *in-situ* observation of consolidation flow, which serves as the basis for constructing a consolidation model, thus informing the likelihood of porosity. The important factor in designing the process is tailoring the consolidation parameters to the resin rheo-kinetics and the compaction behaviour of the preforms. Depending on the resin state during consolidation, the pressure in resin, and hence the associated flow mechanisms, can be drastically different. The resin needs to bear higher pressures than the hosting preform so that both air dissolution and mobility are enabled. On the other hand, it must be sufficiently fluid to fill the air pockets and for a preform to conform with the required thickness. This study, therefore, characterises a fast-curing resin system used for injection, using real-time monitoring, and derives the response of the locally impregnated fabric. Manufacturing trials examine the relationship between the consolidation parameters and the resulting porosity to validate the modelling approach.

Finally, trials with a functionalised resin are described to showcase the feasibility of such processes for local, filler-modified resins and their potential applications. As a result, the paper delivers a practical model-based and trial-driven methodology for creating high-quality multi-matrix composite systems using a novel resin injection method. The deployment of fast-curing resin systems and tailoring process parameters to resin rheo-kinetics allows for paving the way for quick and efficient patch creation, which is essential for the industrial deployment of this technique.

2. MATERIAL SYSTEMS AND CHARACTERISATION

2.1 Material selection

The selection of the resin plays a vital role both as the primary matrix and as a carrier for functional additives in patch integration. The selected materials and key properties are summarised in Table 1.

A fast-curing resin system offers several significant advantages for localised processes. Firstly, current fast-cure resins can be fully cured in a timescale of minutes and hence, the patch integration will not significantly increase the length of the entire manufacturing process. Secondly, owing to the short curing timescales at higher temperatures, these resins can be rapidly tuned to move from low to high DOC, in turn increasing the viscosity in orders of magnitude, which allows flexible control of the manufacturing process. Finally, the selected resin needs to have a low viscosity at injection to easily impregnate the fabric and high latency at room temperature to ensure longer pot life. The liquid resin system selected for this study was a bisphenol A diglycidyl ether (DGEBA) based epoxy, Araldite 3585, and a cycloaliphatic polyamine

hardener, Aradur 3475. The gel time drops by 96% on increasing the temperature from 40°C to 110°C, which is indicative of a latent fast-cure epoxy system.

Table 1 Materials used and their properties.

Liquid resin system (Huntsman Advanced Materials)					
Name	Mix Ratio	Viscosity at 25°C	Pot life at 25°C	Gel time at 40°C	Gel time at 110°C
Araldite 3585/ Aradur 3475	100:21	0.9 Pa·s	25-35 min	50 min	2 min
Fabric (Saertex)					
Fibre	Architecture	Fibre density	Areal density	Stitch density	
E-glass	NCF	2.55 g/cm^3	450 gsm	6 gsm	
Diluent (Sigma-Aldrich)					
Name	Density	Molecular weight	Viscosity at 25°C		
glycidyl 2-methylphenyl ether	1.079 g/cm^3	164.2 g/mol	5-10 mPa·s		
Functional powdered additive (Imperial College London)					
Material	Araldite GT7071	Dyhard 100S	NC7000 (Nanocyl)		
Type	DGEBA powder epoxy	Dicyandiamide solid curing agent	Multi-walled CNT		
Content	81.6 wt.%	3.4 wt.%	15.0 wt.%		

A cryomilled, multi-walled carbon nanotube (CNT) enhanced epoxy powder developed at Imperial College London [37] was used as a functional powdered additive to showcase the potential of the process to improve through-thickness electrical conductivity. The baseline liquid resin, Araldite 3585, was modified using 10 and 20 wt.% cryomilled powder to form two formulations modified with 1.5 and 3.0 wt.% effective CNT content, respectively. The two formulations were further modified with 20 wt.% diluent to counter the increase in viscosity associated with the addition of CNT. The diluent used was glycidyl 2-methylphenyl ether, an aromatic mono epoxide. The

addition of 15 wt.% of similar monofunctional diluent has been shown to reduce the viscosity of the neat epoxy system by 95% [38]. The hardener ratio was modified to the epoxide content in the formulations and was 19.89 and 19.95 in every 100 parts of the 1.5 and 3 wt.% CNT modified resin, respectively.

A non-crimp fabric (NCF) was chosen for this study as, by design, such an architecture is optimised to provide a balance between the drapeability of woven fabrics and an in-plane performance of unidirectional (UD) fibres.

2.2 Rheo-kinetics of the resin system

The monitoring of the resin viscosity during the injection and consolidation processes plays an essential role and needs to be described by a flexible rheo-kinetic model that captures the complex thermal history of the process. The rheo-kinetic modelling used in this study is based on the approach developed by Kiuna *et al.* [32]. The input for the model was provided by rheological measurements using a TA Instruments Discovery HR-30 hybrid rheometer with disposable 25 mm diameter aluminium parallel plates and equipped with a furnace chamber for temperature control. Each sample was prepared by weighing out 10.0 g of resin and 2.1 g of hardener into a 10 ml syringe to meet the prescribed stoichiometric ratio and was mixed with a stirrer.

The isothermal evolution of viscosity was observed by testing three samples, each at six different temperatures ranging from 40°C to 90^{o}C (representative of the processing conditions) at each 10^{o}C interval. Before the tests, the samples were loaded into the pre-heated furnace leading to an initial temperature drop of 5^{o}C due to the

sample setting operation. The oscillating plates were then lowered to hold a 1 mm gap and an oscillation frequency of 10 rad/s was applied. An amplitude sweep at room temperature was conducted to identify the linear viscoelastic region (LVR) and the mean storage modulus was found to be (0.32±0.10) Pa in the strain region from 4% to 60%. Hence, a strain of 5% which lies within the LVR was chosen for the isothermal rheology experiments. An independent validation test was conducted at the same oscillation frequency and strain to observe the viscosity evolution during a complex multi-stage thermal history. The chosen thermal history was derived directly using a thermocouple placed close to the patch in the middle of a four-ply preform stack from a trial run of the cure and consolidation setup and hence representative of the cycle for processing multi-matrix composites in the lab settings: from the point of mixing, through to injection, and finally culminating with thermal conditioning and consolidation.

Due to the highly reactive nature of the resin, the crosslinks were formed before thermal equilibrium was achieved. Hence, the initial viscosity of the resin at a given temperature, the information required for full rheological description, is uncertain and is subject to high noise. Therefore, to estimate the initial viscosity reliably, the viscosity-time relation from a stable part of the measurements was extrapolated to the initial stage of the test. An analytical function in the form of a reduced Prony series was used to approximate viscosity as a function of time for each of the isothermal tests and then extrapolated to the start of the test (Figure 1).

The fitting of these parameters, determined for each isothermal test by bi-square weights regression, is satisfactory, with an R^2 value of 0.98 for every case. The initial

viscosity η_0 was then derived from the obtained fit for the time corresponding to the start of the test. The obtained dependency of initial viscosity to the temperature is well described by Arrhenius-based dependence $\eta_0(T) = A_1\, exp\left(\frac{E_1}{RT}\right)$, where *R* is the ideal gas constant, A_1 and E_1 are the material constants.

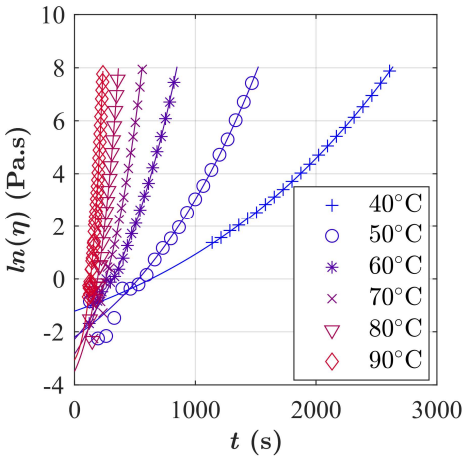

Figure 1 Prony series fit (line) to experimental (discrete markers) isothermal viscosity measurements to estimate the viscosity at *t = 0* at various temperatures

The rate of advance of the cure for a given temperature in Equation (1), *k(T)*, can be determined by examining $\beta(\tau, T)$ and finding the time required to reach $\beta = 1$ in each isothermal case. The resultant data points can be well described by the Arrhenius type function: $k(T) = A_2\, exp\left(\frac{-E_2}{RT}\right)$. The experimentally determined *ln k* can be plotted against the inverse of temperature to fit the parameters A_2 and E_2. The following expression for the master curve, like the dependence observed for Derakane Momentum 411-C50 epoxy resin [32], was used to fit the obtained data. The functions $g(T)$ and $\beta(T)$ take the form in Equation (2).

$$\beta = G_1(T)\left[exp\left(\frac{\tau}{G_2(T)}\right) - 1\right] \quad g = G_2(T)\left(G_1(T)\, exp\left(\frac{\tau}{G_2(T)}\right)\right)^{-1} \qquad (2)$$

Where G-functions can be adequately approximated through trial and error as $G_1 = E_4 - A_4 T$ and $G_2 = A_3\, exp\left(\frac{E_3}{RT}\right)$, where E_3, A_3, E_4 and A_4 are material parameters that are identified using non-linear least square regression analysis with a least absolute residuals (LAR) method. Both the Arrhenius fit for the rate factor term and $\beta(\tau, T)$ function were good with an R^2 value of 0.99 (Figure 2). Thus, all eight of the rheo-kinetic parameters were determined with acceptable accuracy (Figure 2).

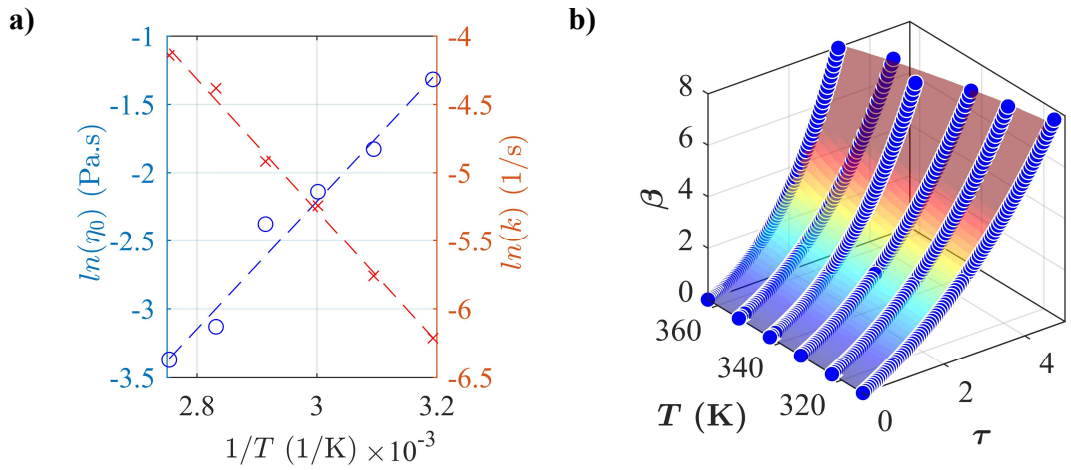

Figure 2 a) Arrhenius fit of initial viscosity (blue), $\boldsymbol{\eta_0}$ and rate factor (red), $\boldsymbol{k}$ and b) surface fit to identify the terms $E_{3\text{-}4}$ and $A_{3\text{-}4}$ in $\boldsymbol{\beta/T/\tau}$ space (discrete points – experimental data).

These parameters indeed give a satisfactory fit for the viscosity in isothermal tests. The comparison between the predicted and the experimental viscosity for a complex thermal history is validated in Figure 3. The overall prediction is close to the measured viscosity throughout the cycle with an R^2 value of 0.97. The model can therefore be confidently used for predicting viscosity evolution in complex thermal programmes.

Table 2 The identified modelling parameters of the rheo-kinetic model.

A_1 (Pa·s)	E_1 (J/mol)	A_2 (Pa·s)	E_2 (J/mol)
8.34×10^{-8}	39054	9754	40088
A_3 (-)	E_3 (J/mol)	A_4 (1/K)	E_4 (-)
0.165	7608	0.029	12.800

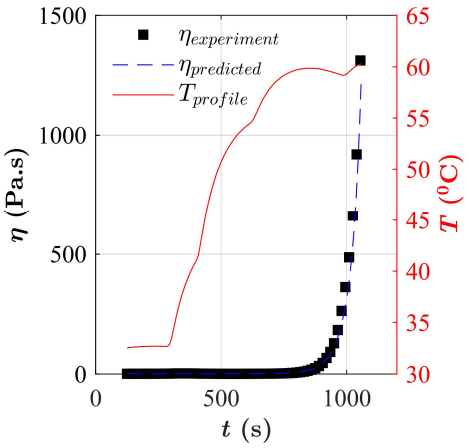

Figure 3 Complex thermal history curing for validating the quality of the model.

2.3 Fabric Compaction Response

The compaction rig consisted of a Zwick universal testing machine with a 100 kN load cell equipped with flat, self-aligning circular platens of 120 mm radius was used to compress square preform samples. Machine compliance was assessed independently by conducting a blank test with no sample. The samples were made up of 4 plies of 100 mm square preform with a $[45/-45]_{4s}$ stacking sequence. A displacement-controlled compaction test was conducted at 40 mm/min to a load of 12 kN and the compaction force and displacement were recorded. The machine displacement measured was subtracted from the corresponding displacement measured during the compaction test

to determine the actual compaction response of the sample. The volume fraction of the fabric, f, can then be expressed as $f = \frac{N}{h}\frac{A_\rho}{\rho}$, where N is the number of plies, A_ρ is the experimentally measured areal density of a ply, ρ is the density of fibre and h is the thickness at any given load, which corresponds directly to the displacement measured.

3. CONSOLIDATION EXPERIMENTS TO SUPPRESS VOIDS

3.1 Process Description

The liquid resin printing (LRP) used to integrate the functional matrix applies a series of localised injections of reactive resin through-thickness of a dry preform. To suppress the voidage formed at the injection stage, the process parameters in consolidation, such as consolidation pressure, pressure ramp rate and temperature, need to be harmonised with the material state parameters, such as resin viscosity and preform architecture. To investigate this relation, a consolidation setup consisting of a transparent glass base mounted on a testing machine was used, as shown in Figure 4. The resin flow was observed through the base plate during the consolidation process.

The remaining dry area of the preform with a fully cured patch was infused with resin using conventional vacuum-assisted resin infusion [7,8]. The infusion resin used was Prime 20LV (Gurit) with a slow hardener. This infusion resin was chosen for its low viscosity and convenient handling to showcase the feasibility of multi-matrix fabrication; however, the choice is not central to the subsequent discussions on patch manufacturability. The infused preform was then cured for 6 h at 70°C to form a multi-matrix composite. A schematic of the whole process is shown in Figure 5.

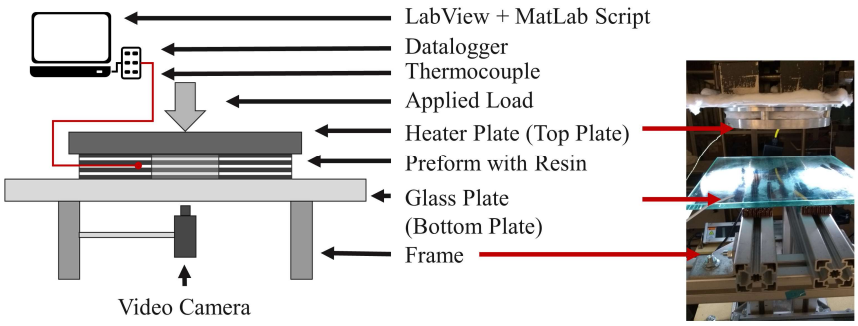

Figure 4 The bespoke consolidation setup with a transparent bottom plate, top heater plate and provision for observing the flow through the preform using a video camera.

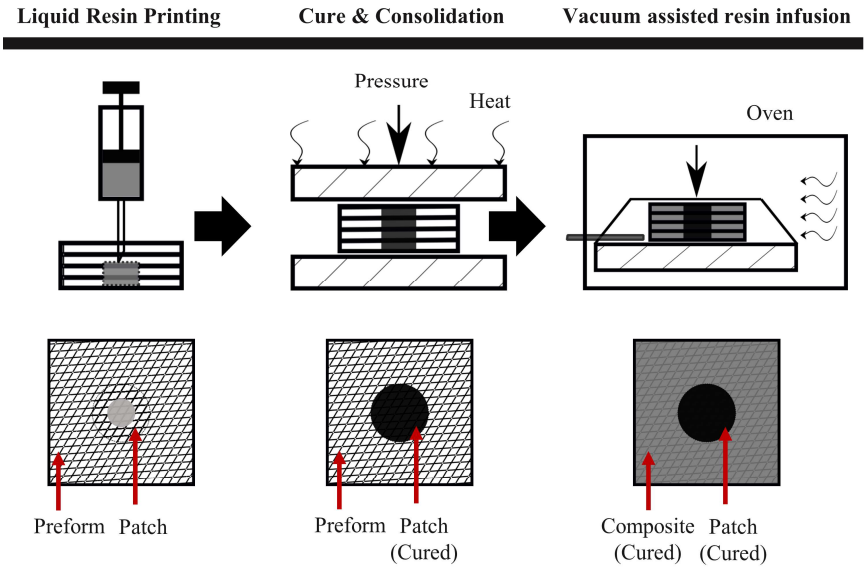

Figure 5 Schematic overview of the manufacturing of multi-matrix composites

3.2 Flow observations

The *in-situ* recordings of the resin flow captured substantial differences in deformation mechanisms at the three different stages of the consolidation process. Before consolidation, an 18-20 mm radius patch is observed (Figure 6), where the resin would predominantly be accumulated within the fibre bundles as the flow is dominated by capillary effects during the injection process [5].

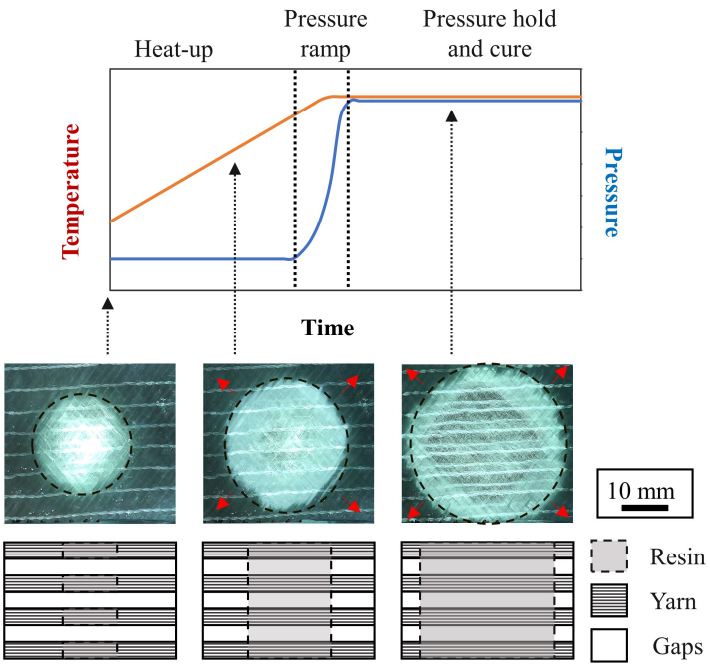

Figure 6 Characteristic resin flow in the patch during the cure and consolidation stage in neat resin trial (low activation viscosity)

During the initial pre-heating stage, the resin started to flow even before consolidation (Figure 6). This flow can be related to the decrease in resin viscosity with temperature, which facilitates capillary flow, combined with the initial force applied to bring the platen in contact with the preform to improve heat transfer. However, this type of flow is observed to cease in the later stages as crosslinking starts to dominate the viscosity of the resin. Once pressure is applied, the resin flow under consolidation becomes visible. The resin flows through the preform and the patch expands in size. The resultant patch morphology differs based on the activation viscosity of the sample and can be classified into two broad types: the low (0.1-10 Pa·s) and high (> 600 Pa·s) pressure response (Figure 7).

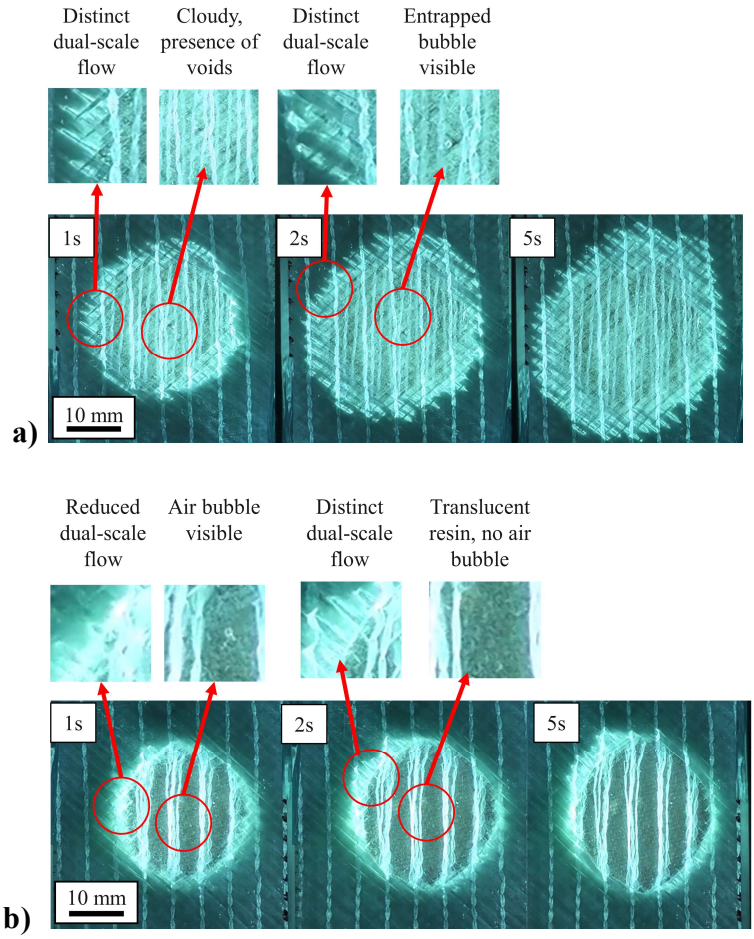

Figure 7 Characteristic evolution of the patch with time stamps indicating time from initiation of pressure ramp for (a) low activation viscosity and (b) high activation viscosity

Both high and low-viscosity activation patches exhibit dual-scale flow: along the yarns, as evidenced by jagged boundaries, and from yarns to the intra-yarn space. The resin flows faster along the inter-ply and inter-yarn regions in the patches with lower activation viscosity. However, the extent of dual-scale flow is far lower in the patches with higher activation viscosity. The amount of air entrapped during the initial stage of the pressure ramp was lowered once the ramp was completed and the patch was cured. There is apparent mobility of air bubbles along the inter-yarn and inter-ply gaps from

the central regions of the patches to the boundaries. This transport was not observed for samples with lower activation viscosity and could be attributed to the higher resin pressure gradient from the patch centre to the patch boundary. The air bubbles move from the central region towards the boundaries. Air bubbles may also have dissolved due to the higher resin pressure. However, this effect could not be qualitatively ascertained from the videos.

There is a clear difference in the translucency of the fully cured patches (Figure 8). The change in the translucency of neat epoxy resin is a well-observed phenomenon in the presence of constituents with different refractive indices [39,40].

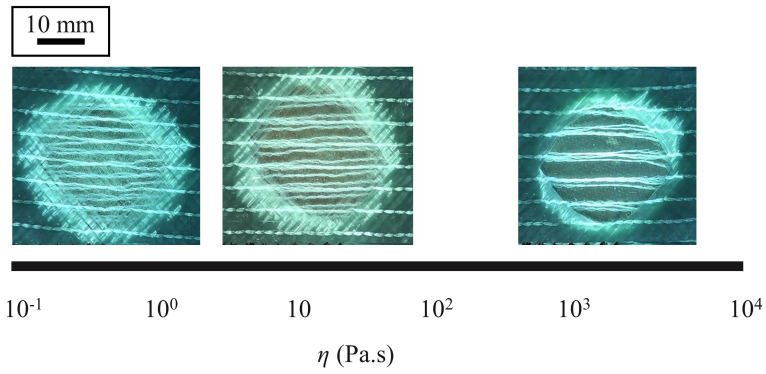

Figure 8 Final patch morphology indicating improved translucency with increasing activation viscosity of the samples observed from flow visualisation setup.

As the glass fibre and epoxy resin have similar refractive indices of 1.55 [41] and 1.59 [42], respectively, the composite should appear translucent. The haziness of the composite may indicate the presence of air bubbles, poor fibre wetting, and other factors [43]. The polyester thread is visible due to a greater mismatch between the refractive indices of the epoxy and polyester. The patches with lower activation viscosity are hazy, whereas the patch with higher initiation viscosity has a clearer central

region. Since air has a significantly different refractive index of 1.003 from the other components, voids likely play a dominant role in controlling the transparency of the composite under different processing conditions.

3.3 Voidage in the patches

The fully infused samples with patches were then cross-sectioned through the centre and examined in two regions: 1) the central region of the patch and 2) the interface between the patch and infused resin (Figure 9).

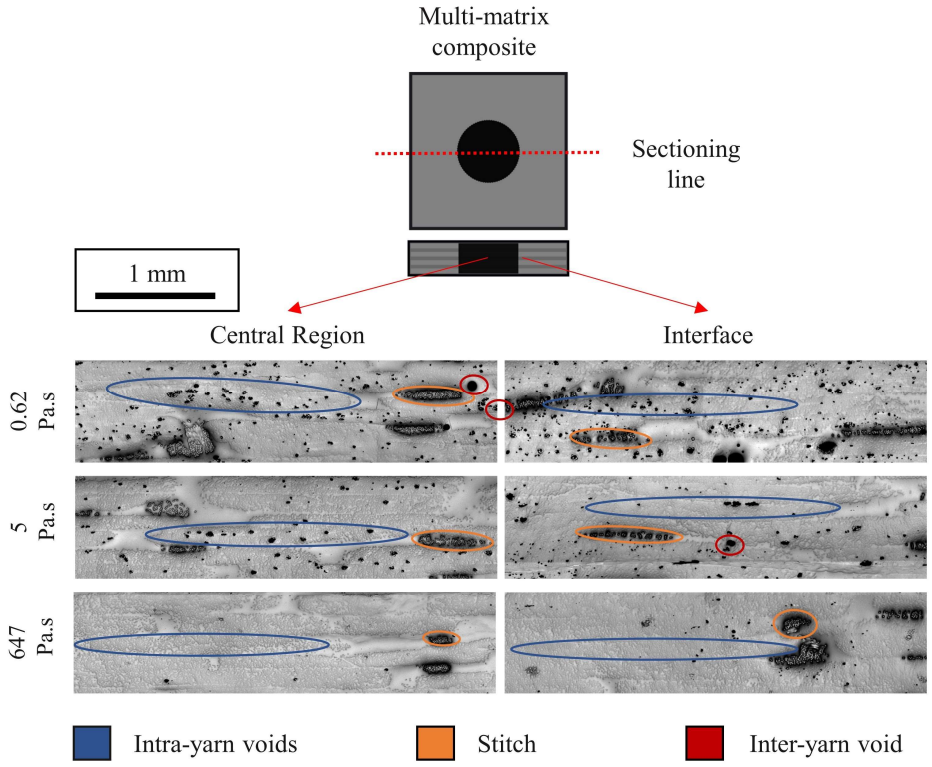

Figure 9 Optical micrographs of the central and interface region of the fully cured patch for various activation viscosities

The void fraction was estimated by processing the optical micrographs using ImageJ by thresholding. In the central region, the void contents were 5.9, 3.8, and 1.1 vol.% for

the activation viscosities of 0.65, 5, and 647 Pa·s, respectively. On increasing the activation viscosity, the void content decreased by 80%. The micrographs quantitatively confirm the qualitative observation of haziness in the flow visualisation studies. In the samples with a lower activation viscosity, a larger fraction of the voids is within the yarns. However, in the samples with higher activation viscosity, the voids are concentrated around the stitch and few voids are present within the yarn. At the interface region, the void contents estimated for these samples were 5.4, 3.4, and 2.9 vol.%, with the highest void content observed for the lowest activation viscosity. The void content is almost the same at the central and interface regions for the samples with lower activation viscosity, while for the higher activation viscosity, the void content is higher at the interface. The increased void content is expected at the interface due to the dual-scale flow during the consolidation of the patches resulting in non-uniform boundary through-thickness. Hence, in the subsequent infusion of the second resin, these cured non-uniform boundaries would inhibit resin flow, causing entrapped voids. This indicates that the viscosity of the second resin could play a critical role in improving the interface quality, however, this was not further investigated in this study.

4. OPTIMISATION OF THE CONSOLIDATION STAGE TO REDUCE VOIDS

4.1 Model development

As seen from the experiments, under the correct processing conditions, the void content in the resin patch could be reduced to as low as 1%. Patch quality can be improved through thermal conditioning; in principle, a suitable flow model for the resin during consolidation will help to optimise the process further. The experiments indicate

a multitude of potential deformations and flow modes, including shear flow and percolation flow both at fibre bundle and patch scales, flow within the yarn openings, yarn-scale capillary flow, deformation of the reinforcement, and void migration. These mechanisms are highly non-linear, coupled and occurring at different scales, and present a serious challenge for a detailed and descriptive analysis. As the material properties of such coupled systems are not known in advance, such modelling may not lead to a straightforward optimisation of process parameters to reduce voids within the patch. Hence, a pragmatic approach was used to navigate the process parameter space by prioritising the two dominant mechanisms observed. At low activation viscosity, the deformation appeared to be dominated by the percolation flow from fibre bundles into the gaps formed by stitching. At high activation viscosity, the flow was defined by the percolation outside of the patch boundary into the dry preform. Even though these two mechanisms do not describe the entire diversity of deformations, they can capture some of the basic process parameters, including resin flow within the patch, patch size evolution, and resin pressure. The percolation model of Gutowski *et al.* [23] was examined as a candidate for the description of both mechanisms but at different structural length scales. The model is based on the additive superposition of the resin pressure resulting from Darcy's flow (viscous response) and the non-linear elastic response of the fibre bed network, P_F. Integrating the mass balance equation and Darcy's flow gives the distribution of resin pressure across the considered volume. The results of these derivations are shown in Table 3.

Table 3 Models for tow-scale and macro-scale flow

Flow Scale	Tow-scale flow (Low Viscosity)	Macro-scale flow (High Viscosity)
Resolving equations	$\eta \frac{df}{dt}\frac{1}{f} = \frac{K_b}{C_b}(P_A - P_F)$	$\eta \frac{df}{dt}\frac{f}{1-f} = \frac{K_m}{C_M}(P_A - P_F)$
Constants	$C_b = \frac{16}{3}\left(\frac{l}{2}\right)^2 \left[1 - \frac{192}{\pi^5}\frac{l}{w}\sum_{n=1,3,5}^{\infty}\frac{1}{n^5} tanh\frac{n\pi w}{2l}\right]$	$C_M = \frac{(1-f_0)}{f_0}\frac{R_0^2}{8}$
Geometrical parameters	$l = 5.0\ mm$ - bundle length $w = 1.7\ mm$ - bundle width	$R_0 = 8\ mm$ - initial radius of the uncompacted patch
Permeability function	$K_b = \frac{k_b\left(\sqrt{\frac{f_m}{f}} - 1\right)^m}{\left(\sqrt{\frac{f}{f_0}} - 1\right)^n}$	$K_m = \frac{k_m\left(\sqrt{\frac{f_m}{f}} - 1\right)^p}{\left(\sqrt{\frac{f}{f_0}} - 1\right)^q}$
Parameters to be identified	k_b, m, n	k_m, p, q
Applied pressure	$P_A = \left(P_{Total}(f) - P_{F,dry}(f)(1 - a_{Patch})\right)/a_{Patch}$	
Known parameters	P_{Total} = Total pressure applied to the preform with resin patch a_{Patch} = Area fraction of the patch in the dry fabric.	
Dry fabric response [44]	$P_{F,dry} = A_{F,dry}\left(\sqrt{\frac{f}{f_{0,dry}}} - 1\right)\left(\sqrt{\frac{f_{m,dry}}{f}} - 1\right)^{-4}$	
Parameters to be identified	$A_{F,dry}, f_{0,dry}, f_{m,dry}, A_F, f_0, f_m$	

The models require a range of input parameters. Some of these parameters occur because of deriving resolving equations, and others come from constitutive

models of permeability or compaction fabric response. As shown by Gutowski et al. [23], the constant C_b appears in derivations when considering force balance: applied pressure is equalised by stresses in the fibre network and the total resin pressure. Integrating the resin pressure ($P_r = P_A - P_F$) over the considered domain results in the constants C_b containing the dimensions of the consolidated area. As pointed out by Gutowski, the resulting expression for tow-scale flow is analogous to the formula for race-tracking region. Constant C_m is derived similarly. The parameters *l* and *w* represent characteristic in-plane dimensions of the impregnated tow before compaction. The length of the fibre bundle within the impregnated patch is dictated by the distance between the stitches, whereas the width is measured directly from preforms images.

The response for dry preform needed for the model was approximated by the well-known formulae of Gutowski et al. [44]. However, since the response of partially in-plane impregnated fabric is different to that measured directly on dry fabric and cannot be directly measured in the context of a rapidly curing resin, the model was fitted as detailed below. A new phenomenological expression for the permeability functions was suggested to reconcile these flow models with the experimental data.

4.2 Parameter identification

The models describing the low and high activation viscosity have six material parameters, each to be identified; the two cases were fitted separately. To obtain the material parameters for the low activation viscosity, the obtained data were plotted in the space of applied pressure, $P_A(f)$, f and normalised rate of fibre volume fraction change: $\eta \frac{df}{dt}\frac{1}{f}$. The six unknown parameters were identified in this space using non-

linear regression. The fabric compaction response parameters identified for the patch should be the same for the high activation viscosity model. Hence, the number of unknown parameters decreases to three parameters, *p*, *q,* and *k*, in the permeability function. Since the fabric compaction response is known, the resin pressure, $P_r = P_A - P_F$ can be calculated from the experimental data. Likewise, the three parameters in the permeability function, $K_m(f)$, were identified using non-linear regression. The parameters for the low activation viscosity were identified with an R^2 value of 0.84 and for the high activation viscosity was identified with an R^2 value of 0.98 (Figure 10). The identified parameters are summarised in Table 4.

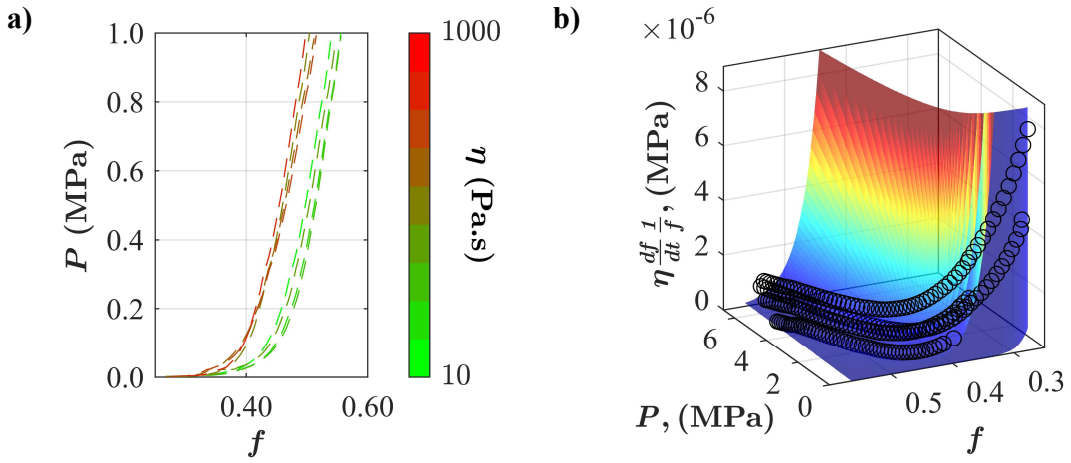

Figure 10 a) Experimental consolidation compaction curves for fabric with resin patches and b) Fit (surface) quality for identifying the material parameters for low viscosity activation flow and the experimental data, which is shown as discrete points.

The material responses identified for the two flow models show several characteristic observations. The dry fabric is stiffer than within the patch, Figure 11(a), where resin lubricates the fibre contacts and, in turn, increases the compressibility of the preform [45]. The yarn permeability is orders of magnitude lower than the macroscale

permeability (Figure 11(b)), as expected, given the permeability of the gap is larger than that of the bundle [46,47].

Table 4 Material parameters identified for the bundle and macro-scale flow models.

Flow Mode	Parameters								
Tow-scale flow (Low Viscosity)	$A_{f,dry}$ (Pa)	$f_{0,dry}$ (-)	$f_{m,dry}$ (-)	A_f (Pa)	f_0 (-)	f_m (-)	m (-)	n (-)	k_b ($m^2 \times 10^{-11}$)
	1873	0.18	0.80	177.20	0.20	0.82	5.77	3.5	11.50
Macro-scale flow (High Viscosity)	$A_{f,dry}$ (Pa)	$f_{0,dry}$ (-)	$f_{m,dry}$ (-)	A_f (Pa)	f_0 (-)	f_m (-)	p (-)	q (-)	k_m ($m^2 \times 10^{-11}$)
	1873	0.18	0.80	177.20	0.20	0.82	1.00	3.5	3.52

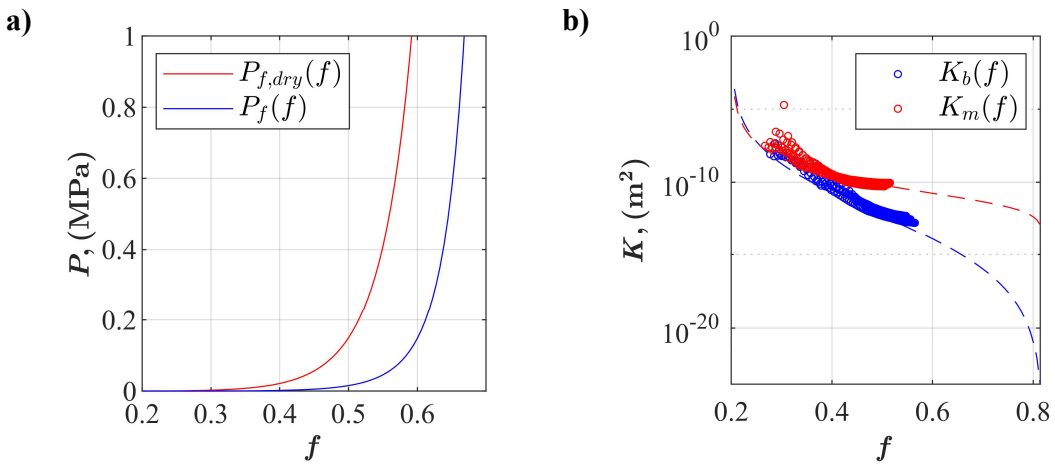

Figure 11 a) Fibre bed response model in dry and patched areas and b) Deduced bundle and macro-scale permeability model along with the experiment (discrete points).

The low and high activation models were then used to estimate the resin pressure at the centre of the patch and correlated with the observed porosity (Figure 12). The resin pressure increases with an increase in activation viscosity while the void content at the centre decreases. The 80% decrease in the void fraction from 5.9 to 1.1

vol.% observed from the micrographs correlates with an estimated increase in resin pressure from 0.16 to 18 MPa, confirming that peak resin pressure and/or pressure gradient across the patch is likely one of the critical factors for dissolving and/or evacuating the voids.

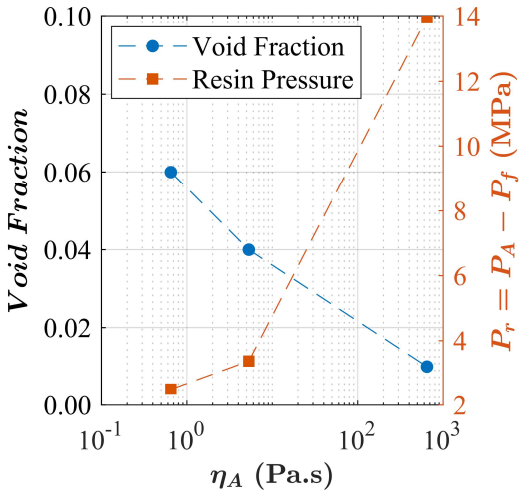

Figure 12 Void fraction (optical micrographs) and resin pressure (model estimations) at the central region of the patch for different activation viscosities.

Typically, mesoscale voids are deemed unacceptable for any composite parts as they are detrimental to mechanical properties [46]. However, micro-scale voids of up to 1% are acceptable for aerospace applications and up to 5% for non-structural applications in other sectors [47]. In the current study, at an activation viscosity of 647 Pa·s, the void content was found to be ~1%, with the voids primarily concentrated deep within the intra-yarn space. In this combination of preform and resin system, the model predicts that a peak resin pressure of 18 MPa is sufficient to reduce the void content to an acceptable region of 1%.

5. FUNCTIONALISATION THROUGH LOCAL INJECTION

The established consolidation methodology was applied to a series of feasibility trials with CNT-modified material within the injection resin. These trials were conducted to explore the potential for improving localised through-thickness conductivity, hence demonstrating a degree of multi-functionality in a multi-matrix composite.

5.1 Process description

The printing procedure for the CNT-modified resin was optimised based on experimental trials. As the viscosity of the resin increased due to the addition of cryomilled powder, the rate of injection was decreased, and the hold increased to account for the slower viscoelastic response. In these experiments, a total of 10 injections of 70 µl/injection were introduced, placed 0.2 mm apart through-thickness into the 4-ply preform, same as the neat resin printing. However, the rate of injection and delay between injections was 700 µl/min, 15 s and 600 µl/min, 17 s for 1.5 and 3 wt.% CNT resin systems, respectively. These parameters had to be altered through trial and error to account for the increased viscoelastic response leading to a delayed response from the injection liquid. A consolidation procedure like the trials with neat resin, which included a pre-heating stage, was adopted. The consolidation stage was then followed by conventional vacuum infusion to form a multi-matrix composite.

5.2 Conductivity measurements

To measure the through-thickness electrical conductivity of the patch regions, two characteristic regions were identified, centre and periphery. The multi-matrix plate was sectioned into 10 mm wide centre and periphery samples. The top and bottom surface was polished to remove a thin layer of insulating resin left from the manufacturing

process resulting in a loss of up to 50 µm on each side. A region of 1 mm in length was then demarcated and the remaining area was masked using tape. This region was then sputter-coated using an Emitech K500X sputter coater with a gold target to form a conductive layer with 0.1 µm thickness to act as a contact surface for conductivity measurements. The thickness of the contact area can be controlled by this method and is uniformly deposited. The electrical resistance was then measured using an Amprobe AM520 two-point probe multimeter. The through-thickness electrical conductivity, σ_{tt} = $h/(A_{ca}R_{\Omega})$), where A_{ca} is the contact area for each case which is 10 mm^2, h is the thickness of each sample and R_{Ω} is the measured electrical resistance. A summary of the results for the representative samples is shown in Table 5.

Table 5 Through-thickness electrical conductivity of characteristic patches

CNT Content	**1.5 wt.%**		**3 wt.%**	
Location	**Periphery**	**Centre**	**Periphery**	**Centre**
Thickness (mm)	1.37	1.48	1.37	1.40
Resistance (kΩ)	106.10	14.22	2.08	2.33
Conductivity (S/m) × 10^{-3}	1.31	10.50	64.70	70.70

In conventional LCM processes, the CNT loadings are typically restricted to 1-2 wt.% due to associated increasing viscosity leading to challenges in good quality infusion which are further exacerbated by the filtration of CNT particles by the fibre network [48–52]. A higher level of loading was achieved in this work due to the localised

introduction of the resin resulting in much shorter flow lengths; hence effects of filtration are limited. The conductivities measured in this study are orders of magnitude higher than values reported for CNT-modified matrix glass fibre-reinforced composites (GFRP) manufactured using other LCM methods and are summarised in Figure 13 [48–52].

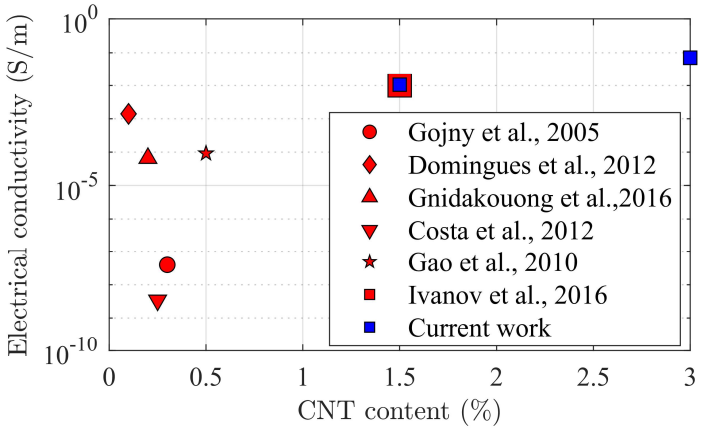

Figure 13 The comparison of through-thickness electrical conductivity vs CNT content used to modify the matrix in GFRP composites in LCM processes in literature and the current study.

The improvements over other reported values reflect the localised nature of the process, combined with the tailored consolidation process. However, earlier work on the functionalisation of GFRP composites using LRP reported conductivities of 9×10^{-3} S/m for CNT loadings of 1.5 wt.%, like the current work [7]. But a larger through-thickness electrical conductivity was possible in this study due to the larger CNT loading of up to 3 wt.% in the printed resin enabled using cryomilled CNT-powder.

The microstructure of the CNT-loaded injected patches was studied by optical microscopy (Figure 14), showing a void content in the centre of the patches of 6 and 15 vol.% for 1.5 and 3 wt.% CNT loadings, respectively.

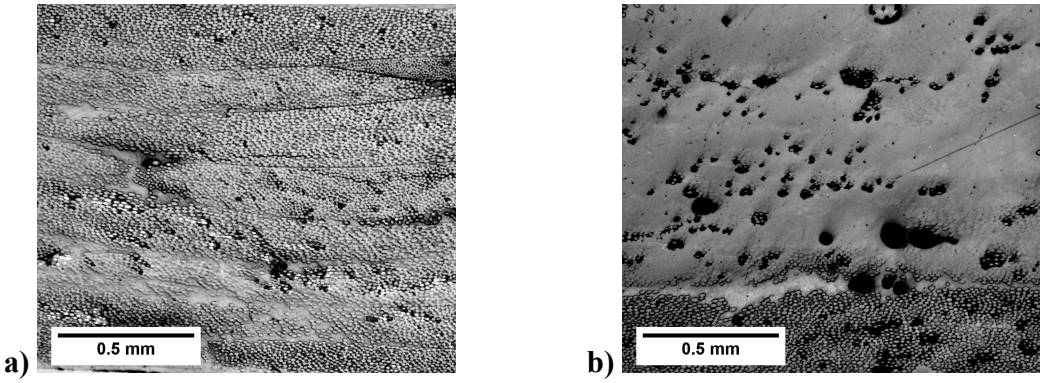

Figure 14 Optical micrographs of the central region of the fully cured patch with a) 1.5 and b) 3 wt.% CNT loadings with voids visible both in the inter – and intra-yarn regions

Despite the acceptable level of electrical conductivity achieved through local processing, the patch quality remains a challenge that needs to be tackled. The optimisation of process parameters for neat resins, as shown in the previous section, yields a clear protocol for void suppression. The void reduction is driven by the optimisation of resin pressure in the centre of the patch and, equivalently, the pressure gradient across the patch area. Given a set of process parameters, the pressure carried by the resin can be increased by increasing its viscosity. The addition of the CNT increases the viscosity of the resin by orders of magnitude effectively to a level beyond that can be provided by advancing the crosslinking of the resin carrier. However, the heterogeneity of the CNT-modified resin triggers additional flow mechanisms which impact the patch quality. Clustering of additives and filtering of clusters at yarn scales impacts flow motion and prevents suppression of the voidage in the same way as seen for the low activation viscosity of the neat resin. These clusters would alter local consolidation by carrying additional pressure leading to non-uniform flow during consolidation.

6. CONCLUSIONS

The current study explores a successful route to an out-of-vacuum bag process with the capability to introduce resin patches for functional and structural applications. Such a process, due to its simplicity and localisation, does not require heavy or expensive manufacturing tools and has the potential to be automated. Implementation would rely on a good understanding of the resin rheo-kinetics and compaction behaviour of the preforms. Good patch quality, *i.e.,* low porosity, can be achieved through optimisation, crucially supported by an appropriate model. The introduction of patches can offer new opportunities to develop and enhance composite properties that are otherwise difficult to obtain. However, the complexity of the deformation and flow mechanisms makes the parameter identification process non-trivial and requires the use of unconventional material response models, such as the permeability-fibre volume fraction functions suggested in this paper. The main route to optimisation lies in increasing the share of the applied pressure in the matrix and shifting it away from the fibre bed. The thermal conditioning of the matrix is a promising mechanism that works particularly well with snap-curing resin systems where the DOC, hence the viscosity, can be advanced rapidly. An alternative method to increase the viscosity of the resin, including the addition of functional fillers (CNTs), was trialled. This route proved useful in improving the through-thickness electrical conductivity. However, more insights are required for such highly heterogeneous resin formulations as the interactions between preform and resin are more complicated. Overall, the obtained results show a good basis for developing direct patch injection technology for multi-matrix composites and present the initial

framework to investigate the process methodology further. This framework consists of developing a rheo-kinetic model, understanding the compaction response of the dry preform and combining these experiments to parametrise the consolidation scheme to be applied for a range of injectable resins.

ACKNOWLEDGMENT

The work has been supported by the EPSRC through the ACCIS Doctoral Training Centre [EP/G036772/1]. This work was also supported by the EPSRC through the Future Composites Manufacturing Research Hub [EP/ P006701/1] as part of the Core Project "Manufacturing for structural applications of multifunctional composites".

DATA AVAILABILITY STATEMENT

All data to support the conclusions reached are included in full in this article. Supplementary data used for rheo-kinetic modelling, fabric compaction, and printed patch consolidation response are available at the University of Bristol data repository: https://doi.org/10.5523/bris.3vjlolgemmsza2m65dovn8gyah

NOMENCLATURE

A	Area
A_{ca}	Contact area
$A_{F,dry}$	The spring constant of the dry preform
A_F	The spring constant of the preform with patch
A_ρ	The areal density of fabric
a_{patch}	Area fraction of the patch in the dry fabric.
f	Fibre volume fraction

F	Force
f_0	The initial fibre volume fraction of the fabric with resin
f_m	Maximum limit on the fibre volume fraction of the fabric with resin
$f_{0,dry}$	The initial fibre volume fraction of the dry preform
$f_{m.dry}$	Maximum limit on the fibre volume fraction of the dry preform
h	Thickness
k	Function expressing cure rate advance with temperature
K	Permeability
K_b	Fibre tow/bundle permeability
K_m	Macroscale permeability of the preform
l	Fibre bundle length
N	Number of plies in a preform
P	Pressure
P_{Total}	Total pressure applied to the preform with resin patch
P_A	Applied pressure
P_F	Effective stress carried by the fabric
R_Ω	Electrical resistance
T	Temperature
t	Time
w	Fibre bundle width
α	Degree of cure (DOC)
β	The viscosity of resin normalised to its initial viscosity at a given temperature
η	Viscosity
η_0	The initial viscosity of resin for a given temperature

ρ Density of material

σ_{TT} Through-thickness electrical conductivity

τ Time normalised to time when $\beta = 1$

REFERENCES

[1] Swolfs, Y., Verpoest, I., and Gorbatikh, L., 2019, "Recent Advances in Fibre-Hybrid Composites: Materials Selection, Opportunities and Applications," International Materials Reviews, **64**(4), pp. 181–215.

[2] Gnaba, I., Legrand, X., Wang, P., and Soulat, D., 2019, "Through-the-Thickness Reinforcement for Composite Structures: A Review," Journal of Industrial Textiles, **49**(1), pp. 71–96.

[3] Qian, H., Greenhalgh, E. S., Shaffer, M. S. P., and Bismarck, A., 2010, "Carbon Nanotube-Based Hierarchical Composites: A Review," J Mater Chem, **20**(23), p. 4751.

[4] Valorosi, F., De Meo, E., Blanco-Varela, T., Martorana, B., Veca, A., Pugno, N., Kinloch, I. A., Anagnostopoulos, G., Galiotis, C., Bertocchi, F., Gomez, J., Treossi, E., Young, R. J., and Palermo, V., 2020, "Graphene and Related Materials in Hierarchical Fiber Composites: Production Techniques and Key Industrial Benefits," Compos Sci Technol, **185**(July 2019), p. 107848.

[5] Ivanov, D. S., White, J. A. P., Hendry, W., Mahadik, Y., Minett, V., Patel, H., and Ward, C., 2015, "Stabilising Textile Preforms by Means of Liquid Resin Print: A Feasibility Study," Advanced Manufacturing: Polymer and Composites Science, **1**(1), pp. 26–35.

[6] Turk, M. A., Vermes, B., Thompson, A. J., Belnoue, J. P. H., Hallett, S. R., and Ivanov, D. S., 2020, "Mitigating Forming Defects by Local Modification of Dry Preforms," Compos Part A Appl Sci Manuf, **128**(July 2019), p. 105643.

[7] Ivanov, D. S., Le Cahain, Y. M., Arafati, S., Dattin, A., Ivanov, S. G., and Aniskevich, A., 2016, "Novel Method for Functionalising and Patterning Textile Composites: Liquid Resin Print," Compos Part A Appl Sci Manuf, **84**, pp. 175–185.

[8] Stanier, D., Radhakrishnan, A., Gent, I., Roy, S. S., Hamerton, I., Potluri, P., Scarpa, F., Shaffer, M., and Ivanov, D. S., 2019, "Matrix-Graded and Fibre-Steered Composites to Tackle Stress Concentrations," Compos Struct, **207**(August 2018), pp. 72–80.

[9] Anthony D.B., Turk M.A., Nguyen S.N., Kucernak A.R , Shaffer M.S., Ivanov D.S., G. E. S., 2020, "Formable Structures for Carbon Aerogel Infused Carbon Fibre Samples," *Proceedings of ECCM19*, Nantes, France.

[10] BK. Fink and McKnight, S.H, Gillespie, J. W., 1998, "Co-Injection Resin Transfer Molding for Optimization of Integral Armor.," Proceedings of Army Science Conference, Norfolk, VA, 1998.

[11] Krollmann, J., Alvarado, C. S., Carqueville, P., Snajdr, R., Zaremba, S., and Drechsler, K., 2016, "Hybrid-Matrix Processing: How to Co-Inject Multiple Resin Systems into One Composite Part ?," *ECCM17 -17th European Conference on Composite Materials*, Munich, pp. 26–30.

[12] Mehdikhani, M., Gorbatikh, L., Verpoest, I., and Lomov, S. V., 2019, "Voids in Fiber-Reinforced Polymer Composites: A Review on Their Formation, Characteristics, and Effects on Mechanical Performance," J Compos Mater, **53**(12), pp. 1579–1669.

[13] Leclerc, J. S., and Ruiz, E., 2008, "Porosity Reduction Using Optimised Flow Velocity in Resin Transfer Molding," Compos Part A Appl Sci Manuf, **39**(12), pp. 1859–1868.

[14] Wood, J. R., and Bader, M. G., 1994, "Void Control for Polymer-Matrix Composites (1): Theoretical and Experimental Methods for Determining the Growth and Collapse of Gas Bubbles," Composites Manufacturing, **5**(3), pp. 139–147.

[15] Bernet, N., Michaud, V., Bourban, P. E., and Manson, J. A. E., 1999, "Impregnation Model for the Consolidation of Thermoplastic Composites Made from Commingled Yarns," J Compos Mater, **33**(8), pp. 751–772.

[16] Zhang, D., Heider, D., and Gillespie, J. W., 2017, "Void Reduction of High-Performance Thermoplastic Composites via Oven Vacuum Bag Processing," J Compos Mater, **51**(30), pp. 4219–4230.

[17] White, S. R., and Kim, Y. K., 1996, "Staged Curing of Composite Materials," Compos Part A Appl Sci Manuf, **27**(3), pp. 219–227.

[18] Lundström, T. S., 1997, "Measurement of Void Collapse during Resin Transfer Moulding," Compos Part A Appl Sci Manuf, **28**(3), pp. 201–214.

[19] Pham, X. T., and Trochu, F., 1999, "Simulation of Compression Resin Transfer Molding to Manufacture Thin Composite Shells," Polym Compos, **20**(3), pp. 436–459.

[20] Gutowski, T. G., Cai, Z., Bauer, S., Boucher, D., Kingery, J., and Wineman, S., 2016, "Consolidation Experiments for Laminate Composites," http://dx.doi.org/10.1177/002199838702100705, **21**(7), pp. 650–669.

[21] Koptelov, A., Belnoue, J. P. H., Georgilas, I., Hallett, S. R., and Ivanov, D. S., 2022, "Adaptive Real-Time Characterisation of Composite Precursors in Manufacturing," Front Mater, **9**.

[22] Koptelov, A., Belnoue, J. P. H., Georgilas, I., Hallett, S. R., and Ivanov, D. S., 2022, "Revising Testing of Composite Precursors – A New Framework for Data Capture in Complex Multi-Material Systems," Compos Part A Appl Sci Manuf, **152**, p. 106697.

[23] Gutowski, T. G., Morigaki, T., and Zhong Cai, 1987, "The Consolidation of Laminate Composites," J Compos Mater, **21**(2), pp. 172–188.

[24] Hubert, P., and Kratz, J., 2021, "Tool Interface Pressure during the Forming of Model Composite Corners," Compos Part A Appl Sci Manuf, **151**, p. 106639.

[25] Hubert, P., and Poursartip, A., 2001, "Aspects of the Compaction of Composite Angle Laminates: An Experimental Investigation," J Compos Mater, **35**(1), pp. 2–26.

[26] Hubert, P., and Poursartip, A., 1998, "A Review of Flow and Compaction Modelling Relevant to Thermoset Matrix Laminate Processing," Journal of Reinforced Plastics and Composites, **17**(4), pp. 286–318.

[27] Roller, B., 1975, "Characterisation of the Time-Temperature-Viscosity Behavior of Curing B-Staged Epoxy Resin," Polym Eng Sci, (6).

[28] Williams, M. L., Landel, R. F., and Ferry, J. D., 1955, "The Temperature Dependence of Relaxation Mechanisms in Amorphous Polymers and Other Glass-Forming Liquids," J Am Chem Soc, **77**(14), pp. 3701–3707.

[29] Mijovic, J., and Lee, C. H., 1989, "Modeling of Chemorheology of Thermoset Cure by Modified WLF Equation," J Appl Polym Sci, **37**(4), pp. 889–900.

[30] Karkanas, P. I., and Partridge, I. K., 2000, "Cure Modeling and Monitoring of Epoxy/Amine Resin Systems. II. Network Formation and Chemoviscosity Modeling," J Appl Polym Sci, **77**(10), pp. 2178–2188.

[31] Castro, J. M., and Macosko, C. W., 1982, "Studies of Mold Filling and Curing in the Reaction Injection Molding Process," AIChE Journal, **28**(2), pp. 250–260.

[32] Kiuna, N., Lawrence, C. J., Fontana, Q. P. V., Lee, P. D., Selerland, T., and Spelt, P. D. M., 2002, "A Model for Resin Viscosity during Cure in the Resin Transfer Moulding Process," Compos Part A Appl Sci Manuf, **33**(11), pp. 1497–1503.

[33] Lucio, B., and de la Fuente, J. L., 2014, "Rheological Cure Characterization of an Advanced Functional Polyurethane," Thermochim Acta, **596**, pp. 6–13.

[34] Keller, A., Masania, K., Taylor, A. C., and Dransfeld, C., 2016, "Fast-Curing Epoxy Polymers with Silica Nanoparticles: Properties and Rheo-Kinetic Modelling," J Mater Sci, **51**(1), pp. 236–251.

[35] Geissberger, R., Maldonado, J., Bahamonde, N., Keller, A., Dransfeld, C., and Masania, K., 2017, "Rheological Modelling of Thermoset Composite Processing," Compos B Eng, **124**, pp. 182–189.

[36] Keller, A., Masania, K., Taylor, A. C., and Dransfeld, C., 2016, "Fast-Curing Epoxy Polymers with Silica Nanoparticles: Properties and Rheo-Kinetic Modelling," J Mater Sci, **51**(1), pp. 236–251.

[37] Herceg, T. M., Yoon, S.-H., Abidin, M. S. Z., Greenhalgh, E. S., Bismarck, A., and Shaffer, M. S. P. P., 2016, "Thermosetting Nanocomposites with High Carbon Nanotube Loadings Processed by a Scalable Powder Based Method," Compos Sci Technol, **127**, pp. 62–70.

[38] Ozeren Ozgul, E., and Ozkul, M. H., 2018, "Effects of Epoxy, Hardener, and Diluent Types on the Workability of Epoxy Mixtures," Constr Build Mater, **158**, pp. 369–377.

[39] Pascual, C., De Castro, J., Schueler, A., Vassilopoulos, A. P., and Keller, T., 2014, "Total Light Transmittance of Glass Fiber-Reinforced Polymer Laminates for Multifunctional Load-Bearing Structures," J Compos Mater, **48**(29), pp. 3591–3604.

[40] Zobeiry, N., Lee, A., and Mobuchon, C., 2020, "Fabrication of Transparent Advanced Composites," Compos Sci Technol, **197**(March), p. 108281.

[41] Dunkers, J. P., Parnas, R. S., G. Zimba, C., Peterson, R. C., Flynn, K. M., Fujimoto, J. G., and Bouma, B. E., 1999, "Optical Coherence Tomography of Glass Reinforced Polymer Composites," Compos Part A Appl Sci Manuf, **30**(2), pp. 139–145.

[42] Rauf, A., Hand, R. J., and Hayes, S. A., 2014, "Modifying the Refractive Index of Epoxy Resins Using Reactive Diluents to Enable Optical Self-Sensing in E-Glass Fibre Composites," Applied Mechanics and Materials, **625**(March), pp. 90–93.

[43] Lin, H., Day, D. E., Weaver, K. D., and Stoffer, J. O., 1994, "Temperature and Wavelength Dependent Transmission of Optically Transparent Glass Fibre Poly (Methyl Methacrylate) Composites," J Mater Sci, **29**(19), pp. 5193–5198.

[44] Gutowski, T. G., Cai, Z., Bauer, S., Boucher, D., Kingery, J., and Wineman, S., 1987, "Consolidation Experiments for Laminate Composites," J Compos Mater, **21**(7), pp. 650–669.

[45] Kelly, P. A., Umer, R., and Bickerton, S., 2006, "Viscoelastic Response of Dry and Wet Fibrous Materials during Infusion Processes," Compos Part A Appl Sci Manuf, **37**(6 SPEC. ISS.), pp. 868–873.

[46] Nedanov, P. B., and Advani, S. G., 2002, "Numerical Computation of the Fiber Preform Permeability Tensor by the Homogenization Method," Polym Compos, **23**(5), pp. 758–770.

[47] Endruweit, A., Zeng, X., Matveev, M., and Long, A. C., 2018, "Effect of Yarn Cross-Sectional Shape on Resin Flow through Inter-Yarn Gaps in Textile Reinforcements," Compos Part A Appl Sci Manuf, **104**, pp. 139–150.

[48] Gojny, F. H., Wichmann, M. H. G. G., Fiedler, B., Bauhofer, W., and Schulte, K., 2005, "Influence of Nano-Modification on the Mechanical and Electrical Properties of Conventional Fibre-Reinforced Composites," Compos Part A Appl Sci Manuf, **36**(11), pp. 1525–1535.

[49] Reia da Costa, E. F., Skordos, A. A., Partridge, I. K., and Rezai, A., 2012, "RTM Processing and Electrical Performance of Carbon Nanotube Modified Epoxy/Fibre Composites," Compos Part A Appl Sci Manuf, **43**(4), pp. 593–602.

[50] Domingues, D., Logakis, E., and Skordos, A. A., 2012, "The Use of an Electric Field in the Preparation of Glass Fibre/Epoxy Composites Containing Carbon Nanotubes," Carbon N Y, **50**(7), pp. 2493–2503.

[51] Gao, L., Chou, T.-W., Thostenson, E. T., Godara, A., Zhang, Z., and Mezzo, L., 2010, "Highly Conductive Polymer Composites Based on Controlled Agglomeration of Carbon Nanotubes," Carbon N Y, **48**(9), pp. 2649–2651.

[52] Gnidakouong, J. R. N., Roh, H. D., Kim, J.-H., and Park, Y.-B., 2016, "In Situ Assessment of Carbon Nanotube Flow and Filtration Monitoring through Glass Fabric Using Electrical Resistance Measurement," Compos Part A Appl Sci Manuf, **90**, pp. 137–146.

FIGURE CAPTIONS LIST

Fig 1 Prony series fit (line) to experimental (discrete markers) isothermal viscosity measurements to estimate the viscosity at t = 0 at various temperatures

Fig 2 a) Arrhenius fit of initial viscosity (blue), η_0 and rate factor (red), k and b) surface fit to identify the terms $E_{3\text{-}4}$ and $A_{3\text{-}4}$ in $\beta/T/\tau$ space (discrete points – experimental data).

Fig 3 Complex thermal history curing for validating the quality of the model.

Fig 4 The bespoke consolidation setup with a transparent bottom plate, top heater plate and provision for observing the flow through the preform using a video camera.

Fig 5 Schematic overview of the manufacturing of multi-matrix composites

Fig 6 Characteristic resin flow in the patch during the cure and consolidation stage in neat resin trial (low activation viscosity)

Fig 7 Characteristic evolution of the patch with time stamps indicating time from initiation of pressure ramp for (a) low activation viscosity and (b) high activation viscosity

Fig 8 Final patch morphology indicating improved translucency with increasing activation viscosity of the samples observed from flow visualisation setup.

TABLE CAPTIONS LIST